Journal of Catalysis 275 (2010) 99–107

Contents lists available at ScienceDirect

Journal of Catalysis

journal homepage: www.elsevier.com/locate/jcat

Olefin hydrogenation by ruthenium nanoparticles in ionic liquid media: Does size matter?

Paul S. Campbell [a], Catherine C. Santini [a,*], François Bayard [a], Yves Chauvin [a], Vincent Collière [b], Ajda Podgoršek [c], Margarida F. Costa Gomes [c], Jacinto Sá [d]

[a] Université de Lyon, Institut de Chimie de Lyon, UMR 5265 CNRS-Université de Lyon-ESCPE Lyon, C2P2, Equipe Chimie Organométallique de Surface, ESCPE 43 Boulevard du 11 Novembre 1918, F-69616 Villeurbanne, France
[b] Laboratoire de Chimie de Coordination, UMR CNRS, 205, route de Narbonne, 31077-Toulouse cedex 04, France
[c] Laboratoire de Thermodynamique des Solutions et des Polymères, Université Blaise Pascal, Clermont-Ferrand, 24 Avenue des Landais, 63177 Aubière, France
[d] CenTACat, School of Chemistry and Chemical Engineering, Queen's University, Stranmillis Road, Belfast, Northern Ireland BT9 5AG, UK

ARTICLE INFO

Article history:
Received 1 June 2010
Revised 19 July 2010
Accepted 21 July 2010

Keywords:
Nanoparticles
Ruthenium
Ionic liquids
Size effect
Selective hydrogenation

ABSTRACT

Tailor-made and size-controlled ruthenium nanoparticles, RuNPs, of three distinct sizes between 1 and 3 nm are generated from the decomposition of (η^4-1,5-cyclooctadiene)(η^6-1,3,5-cyclooctatriene) ruthenium(0) [Ru(COD)(COT)], under H_2 in 1-butyl-3-methylimidazolium bis(trifluoromethanesulphonyl)imide, $C_1C_4ImNTf_2$, by simply varying experimental conditions. Catalytic hydrogenation of 1,3-cyclohexadiene, CYD, and cyclohexene, CYE, in $C_1C_4ImNTf_2$, has been used as a probe for the relationship between size and catalytic performance (activity and selectivity) of RuNPs. To allow comparison between different reactions, all catalytic reaction mixtures were diligently prepared in order that the parameters such as substrate/catalyst and substrate/ionic liquid ratio, and therefore, viscosity and mass transport factors remained constant. It was found that the catalytic activity increases with the NP size, while high selectivity is only observed with the smaller NPs. In addition, the studied RuNPs exhibit a high level of recyclability with neither loss of activity nor significant agglomeration.

1. Introduction

Transition-metal nanoparticles (NPs) of 1–10 nm in size exhibit physicochemical properties intermediate to those of the smallest element from which they can be composed and those of the bulk material [1–3]. In catalysis, the performance (activity and selectivity) of NPs is often said to be related to their size, as this controls the number of corner, edge and face atoms available for adsorption and activation of substrates [4–9]. However, the synthesis of nanoparticles (NPs) with a controlled size in the range of 1–10 nm in order to corroborate this theory is still a challenging issue [10].

The use of ionic liquids (ILs) in NP synthesis has recently become a popular route. The major advantage is that stabilising additives such as ligands, polymers and supports are not required. Also, we can tune the IL moieties and reaction conditions to obtain monodisperse and catalytically active NPs of controlled size [7,11–13]. This is because imidazolium-based ILs exhibit a 3-D organisation in the liquid state due to an extended hydrogen-bond network of ionic channels, coexisting with non-polar domains created by the grouping of lipophilic alkyl chains. Consequently, ILs present specific solvation properties [14]. Polar substrates are preferentially dissolved in polar domains and non-polar compounds in non-polar ones [15]. The non-polar organometallic complex, Ru(COD)(COT), is expected to be concentrated in the non-polar domains of ILs. Therefore, the phenomenon of crystal growth is controlled by the local concentration of Ru(COD)(COT) and consequently limited to the size of the non-polar domains. These play the role of nanoreactors in which the size of ruthenium nanoparticles generated *in situ* can be controlled [13,16,17].

Using NPs formed *in situ* in ILs directly in catalysis offers the opportunity to exploit the distinct physicochemical and solvation properties of these media, resulting in unique activities and selectivities [12,18–21].

When comparing the catalytic activity of differently sized nanoparticles, it is important to maintain constant all other possible variables. Indeed, differences in catalytic activity could have a physicochemical origin [22,23], resulting from peculiar solvation phenomena including specific interactions between the IL and the substrate (H bonds, cation-π) [24–26], mass transfer factors (viscosity, diffusivity) [22,27], and effects attributed to the highly structured nature of ILs [14,28,29].

It has been shown that it is possible to obtain ruthenium nanoparticles, RuNPs, of differing sizes from the decomposition of Ru(COD)(COT) in $C_1C_4ImNTf_2$, by simply varying the experimental conditions [16]. In this work, we use the catalytic hydrogenation

* Corresponding author. Fax: +33 472431795.
E-mail address: santini@cpe.fr (C.C. Santini).

0021-9517/$ - see front matter © 2010 Elsevier Inc. All rights reserved.
doi:10.1016/j.jcat.2010.07.018

of 1,3-cyclohexadiene, CYD, and cyclohexene, CYE, as probes for the relationship between size and catalytic performance of tailor-made and size-controlled RuNPs, generated in the ionic liquid, all other physicochemical variables being constant.

2. Experimental

2.1. Materials and methods

All operations were performed in the strict absence of oxygen and water under a purified argon atmosphere using glovebox (Jacomex or MBraun) or vacuum-line (Schlenk) techniques. The ionic liquid, $C_1C_4ImNTf_2$ [30], and the complex, [Ru(COD)(COT)] [31], were synthesised as reported. The halide content of the ionic liquid was under 200 ppm (E.A.) and water under 5 ppm (limit of Karl Fischer titration). Elemental analyses were performed at the CNRS Central Analysis Department of Solaize.

1-Methylimidazole (>99%) was purchased from Aldrich and distilled prior to use. Chlorobutane (>99%, Aldrich) and lithium bis(trifluoromethanesulfonyl)imide (Solvionic) were used without further purification.

2.2. Catalyst synthesis

A solution of (η^4-1,5-cyclooctadiene)(η^6-1,3,5-cyclooctatriene)ruthenium(0) Ru(COD)(COT) (43 mmol L^{-1}) in the ionic liquid 1-butyl-3-methylimidazolium bis(trifluoromethylsulphonyl)imide ($C_1C_4ImNTf_2$) was transferred under argon to a glass autoclave, the temperature of which was controlled with aid of a thermostatic bath (0, 25, 50 or 75 °C). Once stabilised, the argon atmosphere was evacuated and replaced with molecular hydrogen (4 bar) without stirring. The yellow solution turned black over time (up to 3 days) as RuNPs were generated releasing cyclooctane (COA) as the only by-product. The resulting solutions were treated under dynamic vacuum during a period of 6 h to remove all H_2 and cyclooctane. The black solutions could then be stored under argon atmosphere with long-term stability (at least 6 months – no precipitation, coalescence or agglomeration – verified by TEM).

2.3. Determination of particle size by TEM

Transmission electron microscopy (TEM) experiments were performed directly in the IL media. A thin film of RuNP solution in IL was deposited on a carbon film supported by a copper grid. Conventional TEM micrographs were obtained at the Centre Technologique des Microstructures, Université Claude Bernard Lyon 1, Villeurbanne, France, using a Philips 120 CX electron microscope with acceleration voltage of 120 kV. Size distribution histograms were constructed from the measurement of at least 200 different nanoparticles assuming a near spherical shape and random orientation. High-resolution electron micrographs were obtained at the "TEMSCAN" centre of the Université Paul Sabatier Toulouse 3, Toulouse, France, using a JEOL JEM 200CX electron microscope with acceleration voltage of 200 kV.

2.4. XPS

X-ray photoelectron spectroscopy was performed in a Kratos Axis Ultra DLD spectrometer, using a monochromated Al Kα X-ray with a pass energy of 20 eV and a coaxial charge neutraliser. The base pressure in the analysis chamber was better than 5×10^{-8} Pa. XPS spectra of Ru3p, C1s, Si2p and O1s levels were measured at a normal angle with respect to the plane of the surface. High-resolution spectra were corrected for charging effects by assigning a value of 284.6 eV to the C1s peak (adventitious carbon). Binding energies were determined with an accuracy of ±0.2 eV. The data were analysed using Casa-XPS (v 2.3.13) employing a Shirley background subtraction prior to fitting and a peak shape with a combination of Gaussian and Lorentzian (30% Lorentzian). High-resolution spectra were acquired in the region of Ru 3p as the Ru 3d region overlaps with the C 2p region of the residual ionic liquid.

2.5. Preparation of catalytic experiments

In Table 1 are collected all data concerning the studied hydrogenation reaction. In columns 1–3, size and dispersion values of (**Ru_0**), (**Ru_{25}**) and (**Ru_{50}**) are reported.

Each solution of NP was produced from the decomposition of 43.0 mmol L^{-1} solution of Ru(COD)(COT) as described in Section 2.2 and shown in column 4.

For each different temperature of decomposition, a different size of NP is obtained: at 0 °C, 1.1 nm (**Ru_0**); at 25 °C, 2.3 nm (**Ru_{25}**); and at 50 °C, 2.9 nm (**Ru_{50}**), shown in columns 1 and 2.

The value of dispersion, $\mathscr{D}$, describing the ratio of surface sites **Ru_s** to total number of ruthenium atoms, varies with the NP size and is given for each size of NP in column 3. Using this and the known concentration of ruthenium (43.0 mmol L^{-1}), it is possible to calculate for each size of catalyst the concentration of **Ru_s** (column 5). For example, for **Ru_0** (1.1 nm), we have a dispersion of 82% and therefore a **Ru_s** concentration of 35.2 mmol L^{-1}.

To prepare the catalytic mixtures, we must have the same number of catalyst sites. For this reason, we dilute the most concentrated solutions, i.e. **Ru_0** and **Ru_{25}**, to match the least concentrated, i.e. **Ru_{50}**, by the addition of the appropriate amount of pure IL.

Ru_{50} has a concentration of **Ru_s** of 18.5 mmol L^{-1}. A 5-mL sample of this solution therefore contains 9.52×10^{-5} mol of **Ru_s**.

Ru_{25} has a concentration of **Ru_s** of 22.9 mmol L^{-1}. A 3.74-mL sample of this solution is therefore taken, containing 9.52×10^{-5} mol of **Ru_s**, and then diluted with 1.26 mL of pure IL to make a 5-mL solution.

Ru_0 has a concentration of **Ru_s** of 35.2 mmol L^{-1}. A 2.58-mL sample of this solution therefore contains 9.52×10^{-5} mol of **Ru_s** diluted with 2.42 mL of pure IL to make a 5-mL solution (columns 6–8).

To each of these 5-mL catalyst/IL solutions, weighing 7.0 g (column 9), is added 0.78 g of CYD (column 10). This gives catalytic mixtures with constant substrate/catalyst ratios of 105 (column 11) and constant substrate/IL ratios of 0.59 (column 12) ensuring identical viscosities and a single phase.

Using solutions prepared as described, the reaction is carried out in parallel in several 0.5-mL batches under 1.2 bars of pure molecular hydrogen, which are stirred and heated with the aid of a thermostatic carousel, to ensure identical reaction conditions.

2.6. Catalytic tests

Catalytic solutions were made as described in Section 2.5 in a glove box and left stirring for 12 h in a closed system to ensure homogeneity. Aliquots of 0.5 mL were transferred to identical Schlenk tubes containing cross-shaped magnetic stirrer bars. The argon atmosphere was removed, and the solution was degassed *in vacuo* whilst cooling in liquid nitrogen (−196 °C). For reactions at 30 °C, six of these Schlenk tubes were placed in a thermostatic carousel to ensure identical temperature and stirring conditions. After 30 min, when the temperature had stabilised, the Schlenk tubes were opened to 1.2 bars of H_2. After ***t*** minutes, a Schlenk tube was isolated and opened to air, releasing the H_2 atmosphere thus quenching the reaction. The solution was entirely dissolved in 10 mL of acetonitrile containing a 1 M concentration of toluene.

Table 1
Calculations for the composition of the catalytic systems. Column 1 – name of catalyst, column 2 – average RuNP diameter measured by TEM, column 3 – calculated dispersion, column 4 – initial Ru(COD)(COT) concentration, column 5 – consequent $\mathbf{Ru_s}$ concentration, column 6 – volume of IL/RuNP solution, column 7 – volume of pure IL added, column 8 – consequent number of moles of $\mathbf{Ru_s}$ in the 5 mL mixture, column 9 – mass of IL, column 10 – mass of substrate, column 11 – substrate/catalyst ratio, column 12 – substrate/IL ratio.

1	2 d (nm)	3 D (%)	4 [Ru] (mmol L^{-1})	5 [Ru_s] (mmol L^{-1})	6 Vol. IL–RuNP solution (mL)	7 Vol. IL pure (mL)	8 $\mathbf{Ru_s}/10^{-5}$ (mol)	9 m (IL/g)	10 m (CYD/g)	11 CYD/$\mathbf{Ru_s}$	12 CYD/IL
$\mathbf{Ru_0}$	1.1	82	43.0	35.2	2.42	2.58	9.52	7.0	0.78	105	0.59
$\mathbf{Ru_{25}}$	2.3	53	43.0	22.9	3.74	1.26	9.52	7.0	0.78	105	0.59
$\mathbf{Ru_{50}}$	2.9	43	43.0	18.5	5.00	–	9.52	7.0	0.78	105	0.59

The composition of the mixture was determined by gas-phase chromatography using toluene as the internal standard.

2.7. Product quantification

The products were quantitatively analysed by gas chromatography on a HP-6890 chromatograph equipped with a flame ionisation detector (FID) and a HP-1 (crosslinked methylsiloxane) column (L: 30 m, int: 0.32 mm, film thickness: 0.25 μm). The injector and detector temperature was 270 °C, and the injection volume was 1 μL. The programme was as follows: initial temperature 70 °C for 13.5 min; ramp 40 °C/min to 250 °C, hold 2 min.

2.8. Density and viscosity

The mixtures of IL and CYD at different compositions were prepared gravimetrically following the procedure already described [27]. The viscosity of the mixture was measured at 298.15 K (controlled to within ±0.005 K and measured with the accuracy better than ±0.05 K) using a rolling-ball viscometer from Anton Paar, model AMVn [27]. The overall uncertainty of the viscosity is estimated as ±2.0%. The densities of the mixtures, necessary to calculate the viscosities, were measured in an Anton Paar vibrating tube densimeter model 512 P, at 298.15 K (measured by a calibrated PRT with an accuracy of ±0.02 K). The overall uncertainty of the density is estimated as ±0.01%.

2.9. Solubility

To measure the solubility, 1 mL of the substrate was stirred with the ionic liquid in a closed system at 298.15 K for 12 h and then left to settle for a further 2 h. A 0.1-mL sample of the ionic liquid phase was weighed, and its composition was determined by GC using the procedure described in Section 2.6. Tests were repeated four times for each substrate to guarantee reproducibility.

3. Results and discussion

3.1. Choice of substrate

The substrate investigated is the conjugated diene, 1,3-cyclohexadiene (**CYD**). It has been shown that in ionic liquid media, **CYD** may be partially hydrogenated with high selectivity by molecular catalysts due to the reduced miscibility of cyclohexene (**CYE**) in the medium [27,32,33]. Full hydrogenation would lead to cyclohexane (**CYA**), Scheme 1.

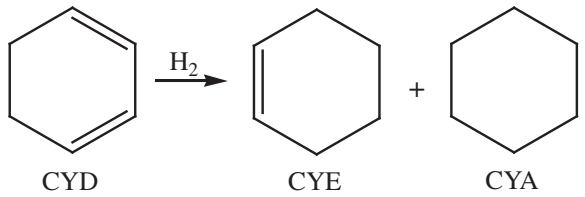

Scheme 1. 1,3-Cyclohexadiene and its hydrogenation products.

3.2. Solubility

The solubilities of the substrate and potential products may play an important role in the activity and/or selectivity of the system. For example, selective hydrogenation of butadiene to butenes has been performed by Dupont's group in ionic liquids due to the difference in solubility of the partially hydrogenated product [34]. The same group has also described the possibility of extracting cyclohexene during benzene hydrogenation using this solubility difference [35]. For this reason, solubilities of **CYD**, **CYE** and **CYA** are measured. It is found that the solubility of the hydrogenated products (6 ± 1% wt – **CYE**, 4 ± 1% wt – **CYA**) is much lower than that of **CYD** (12 ± 2% wt); therefore, the medium may tend to a biphasic system during the course of the reaction. As a result, the collection of aliquots from a single batch would render inaccurate results. Consequently, each point recorded in this work corresponds to a separate experiment, quenched after time ***t*** by opening the reaction vessel to air, thus releasing the hydrogen and dissolving the catalytic system entirely in a 1 M solution of toluene in acetonitrile for gas-phase chromatography.

3.3. Viscosity

Thermophysical properties of the reaction medium such as density and viscosity may also influence the catalytic performance. We have recently demonstrated that reaction kinetics in IL media are highly dependent on the mobility of molecules [27]. Consequently, identical concentrations of substrate must be used in each case in order to maintain constant viscosity and eliminate effects due to mass transport. Furthermore, knowledge of the viscosity is very important from engineering point of view as it plays a major role in stirring, mixing and pumping processes. The densities and viscosities of the pure $C_1C_4ImNTf_2$ and those of the mixtures with CYD were measured at different molar ratio CYD/IL (R) at 25 °C and atmospheric pressure. The results are presented in Table 2.

As can be seen, the viscosity of the mixtures of CYD in IL varies greatly with the concentration of CYD. From the Stokes–Einstein

Table 2
Density, ρ, and viscosity, η, of CYD–IL mixtures of different compositions. x_{IL} = molar fraction of IL, R = molar ratio CYD/IL.

R	x_{IL}	ρ (g cm^{-3})	η (m Pa s)
0.000	1.000	1.4376 ± 0.0001	48.5 ± 0.4
0.100	0.909	1.4202 ± 0.0001	44 ± 1
0.200	0.833	1.3999 ± 0.0001	37.0 ± 0.4
0.300	0.769	1.3874 ± 0.0003	33.3 ± 0.3
0.397	0.716	1.3718 ± 0.0001	31.0 ± 0.3
0.498	0.667	1.3597 ± 0.0001	24.8 ± 0.3

relation, the diffusion coefficient, $\mathscr{D}$, which reflects to the mobility of molecules, varies inversely with η,

$$\mathscr{D} = \frac{kT}{6\pi\eta r_s} \quad (1)$$

3.4. Catalyst characterisation

It has been previously demonstrated that the size of RuNPs generated from the decomposition of [Ru(COD)(COT)] under H_2 [36], may be governed by the degree of self-organisation of the imidazolium-based ionic liquid in which they are formed: the more structured the ionic liquid, the smaller the size [16]. Following previously described methods, RuNPs are synthesised at 0 °C, 25 °C, 50 °C and 75 °C in an attempt to obtain a selection of monodisperse sizes of RuNP in the same IL.

3.4.1. TEM

Analysis of the suspensions obtained by transition electron microscopy allows the determination of the sizes generated: 1.1 ± 0.2 nm, 2.3 ± 0.3 nm, 2.9 ± 0.4 nm and 3.1 ± 0.7 nm, for RuNPs generated at 0 °C (Ru_0), 25 °C (Ru_{25}), 50 °C (Ru_{50}) and 75 °C (Ru_{75}), respectively, Fig. 1. As can be seen from the TEM image of Ru_{75} and the consequent size distribution histogram Fig. 2, the size of these NPs does not vary significantly compared to those of Ru_{50} although a poorer size control (wider distribution) is apparent. For this reason, these NPs are not used in catalytic tests. High-resolution electron microscopy reveals the crystalline nature of the RuNPs formed through elucidation of the crystal planes. The Fourier transform images of the HREM have been exploited and indicate that the interplanar distances match with the hcp crystalline phase of Ru (see Supplementary information). For Ru_0, only a larger NP of ≈2 nm is observed by HREM, probably due to the difficulty in observing the smallest NPs with limited contrast although may be indicative of a lower degree of crystallinity in very small RuNPs, as already observed by reverse Monte Carlo simulations.[37].

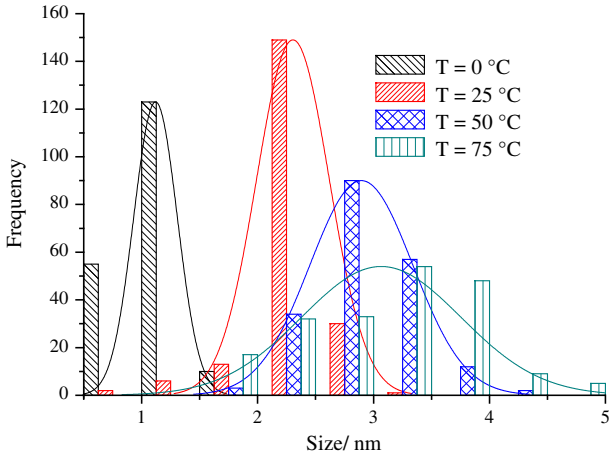

Fig. 2. Comparative size distribution histograms for RuNPs prepared in $C_1C_4Im\ NTf_2$ at different temperatures.

3.4.2. XPS

In order to establish the oxidation state of the RuNPs, X-ray photoelectron spectroscopy (XPS) is performed. Due to the weak

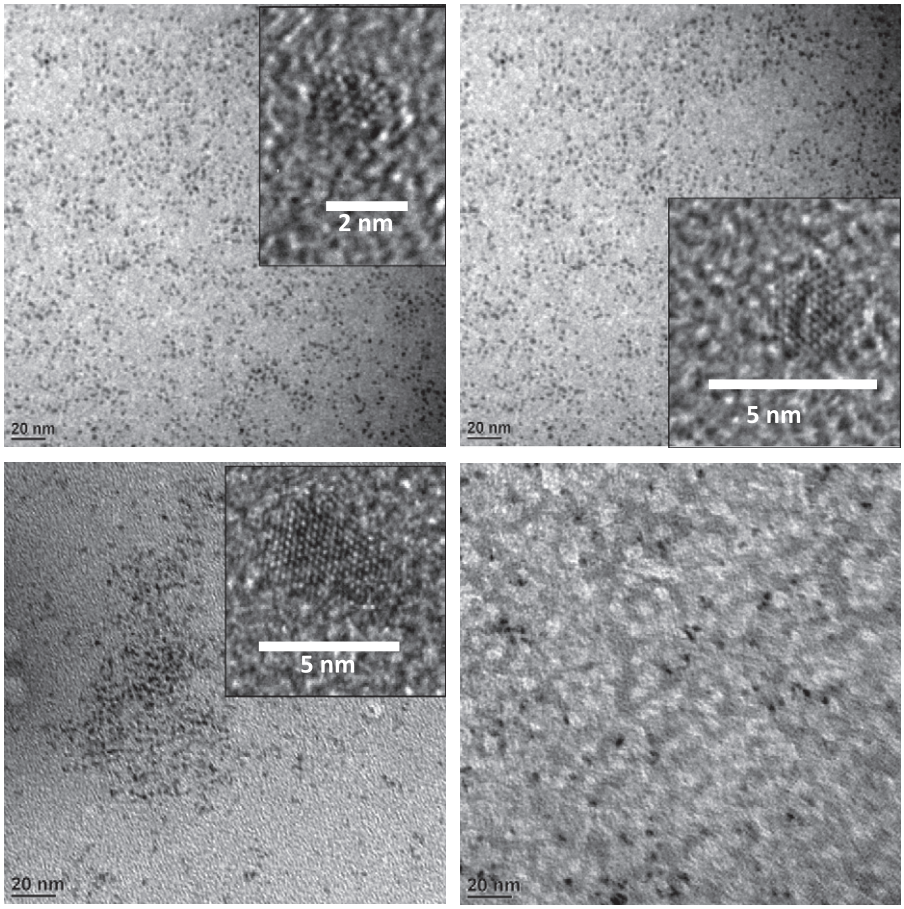

Fig. 1. Transition electron micrograph of RuNPs and high-resolution electron micrograph examples showing crystallinity for Ru_0 (top left), Ru_{25} (top right), Ru_{50} (bottom left) and Ru_{75} (bottom right).

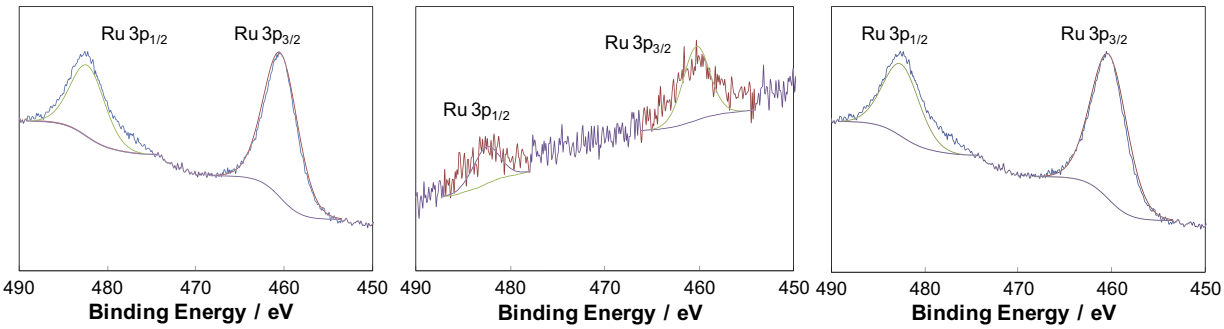

Fig. 3. XPS spectra of the Ru 3p region after NP filtration onto SiO_2, experimental data and fitted peaks. Left **Ru_0**, middle **Ru_{25}** and right **Ru_{50}**.

concentration of the solution and the penetration limit of the X-rays in the solution (maximum depth of 10 nm), no peaks corresponding to Ru binding energies are observed when the analyses are carried out directly on the RuNP/IL solutions. Samples are therefore prepared by filtering the RuNPs onto silica under inert atmosphere and eliminating as much IL as possible. The resulting spectra of the Ru 3p region are depicted in Fig. 3. It is clear that in each case, fine peaks are observed, indicating the presence of only one Ru species. The low $3p_{3/2}$ binding energy observed in each case, 460.3 eV, and doublet separation of 22.2 eV correspond closely to metallic zero-valent ruthenium, often reported with a $3p_{3/2}$ binding energy of around 461 eV [38]. The small difference may be attributed to the presence of small crystallites, which tend to exhibit lower binding energies than bulk metal. Indeed, as recently shown for AuNPs [39], the d band narrows with decreasing particle size and shifts towards the Fermi level.

3.5. Ru_s concentration

Maintaining constant the initial ratio of substrate to catalyst is imperative. In NP catalysis, as in heterogeneous catalysis, only the atoms at the surface (**Ru_s**) take part in reaction. The dispersion ($\mathscr{D}$) presents the ratio between surface atoms, **Ru_s**, and the total number of atoms, **Ru_T**, ($\mathscr{D}$ = **Ru_s/Ru_T**) and varies with the size of the NPs, smaller particles of course having a larger percentage of surface atoms. The different dispersion values must therefore be taken into account for each size of nanoparticle formed.

Ruthenium is known to exhibit a hexagonal close-packed crystal structure, with the following lattice parameters: *a*: 270.59 pm, *b*: 270.59 pm, *c*: 428.15 pm, α: 90°, β: 90°, γ: 120° [40]. Using these parameters, SYBYL software can be applied to extrapolate the lattice until the measured diameters in order to model the structure of the different size NPs, assuming crystallinity. It is seen that crystalline hexagonal close-packed RuNPs would adopt a truncated hexagonal bipyramid form, with two symmetric hexagonal faces (0 0 0 1) and 12 irregular and uneven trapezoid faces (1 0 (−1) 1) [41]. From these findings, a curve of $\mathscr{D}$ with respect to diameter can be plotted and then used to estimate $\mathscr{D}$ for each size of nanoparticle, Fig. 4.

3.6. Catalysis mixture preparation

In Table 2 (Section 2.6) are collected all data concerning the studied hydrogenation reaction. The experimental conditions are established to ensure identical concentrations of **Ru_s** (column 8) and substrate (columns 9 and 10), permitting as a result both a constant substrate/catalyst ratio (column 11) and a constant substrate/IL ratio (column 12) hence constant viscosity. Using solutions prepared as described, the reaction is carried out in parallel

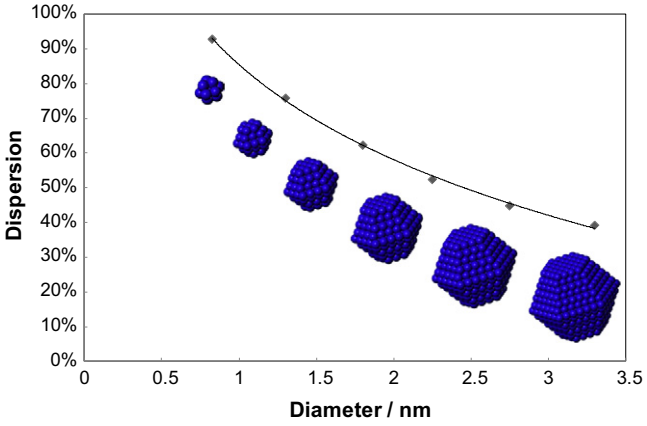

Fig. 4. Curve of dispersion $\mathscr{D}$ against mean diameter of crystalline hcp RuNPs.

in several 0.5-mL batches under 1.2 bars of pure molecular hydrogen, which are stirred and heated with the aid of a thermostatic carousel, to ensure identical reaction conditions.

3.7. Catalytic activity

It can be seen in Table 3 (Experiments 1–3) that the largest NPs (2.9 nm) are the most active in the hydrogenation of **CYD**. In a similar fashion, the three sizes of RuNP are tested in the catalytic hydrogenation of cyclohexene (**CYE**) to cyclohexane (**CYA**) to establish whether a difference in activity is also apparent in the case of a monoene. The results tabulated in Table 4 show that no substantial difference in activity is observed unlike the case of the conjugated diene **CYD**.

In the case of in the catalytic hydrogenation of cyclohexene (**CYE**) to cyclohexane (**CYA**), the TOF value for **Ru_0** is comparable to that reported by Roucoux's group with RuNPs (2.5 nm, TOF = 34) in water in the presence of cyclodextrins [42], although clearly here the experimental conditions are entirely different.

According to literature results, the catalytic activity of NPs depends on their size and generally reaches a maximum for those of around 3 nm [43,44]. Here, only a size effect on activity was observed for the case of **CYD**. The fact that the hydrogenation of **CYD** is faster with larger NPs can be related to two factors:

(1) Larger NPs present the appropriate number of neighbouring surface sites to facilitate the π-bond activation of the conjugated system [45].
(2) Through this π-bonding activation similar to benzene, 1,3-cyclohexadiene would lose part of its resonance energy and react more readily [41].

Table 3
Conversion, selectivity, turnover number and turnover frequency for the hydrogenation of CYD at 30 °C. Experiments 1–3 using 1.2 bar H_2. Experiments 4 and 5 using 4 bar H_2.

Experiment number	Catalyst (nm)	Pressure H_2 (bar)	Conversion at 90 min (%)	Selectivity CYE (%)	TON	TOF (h^{-1})	Size after catalysis (nm)
1	**Ru_0** (1.1)	1.2	66 ± 5	97	70 ± 5	46 ± 3	1.3 ± 0.4
2	**Ru_{25}** (2.3)	1.2	75 ± 5	86	79 ± 5	53 ± 3	2.1 ± 0.5
3	**Ru_{50}** (2.9)	1.2	83 ± 5	80	87 ± 5	58 ± 3	2.7 ± 0.5
4	**Ru_0** (1.1)	4.0	57 ± 5	92	59 ± 5	40 ± 3	–
5	**Ru_{50}** (2.9)	4.0	73 ± 5	80	77 ± 5	51 ± 3	–

Table 4
Conversion, turnover number and turnover frequency for the hydrogenation of CYE at 30 °C under 1.2 bar H_2.

Experiment number	Catalyst (nm)	Conversion at 90 min (%)	TON	TOF (h^{-1})
6	**Ru_0** (1.1)	61 ± 5	64 ± 5	43 ± 3
7	**Ru_{25}** (2.3)	64 ± 5	67 ± 5	45 ± 3
8	**Ru_{50}** (2.9)	67 ± 5	70 ± 5	47 ± 3

The coordination of monoenes such as **CYE** does not necessitate large surfaces, explaining the less pronounced size effect in this case.

3.8. Catalytic selectivity

In the hydrogenation of **CYD**, **CYE** is obtained as the major product. Interestingly, the selectivity for **CYE** diminishes with increasing NP size. Indeed, for **Ru_0**, selectivity for **CYE** is 100% at low conversion and only slightly diminishes at high conversion (97%). In contrast, for **Ru_{50}**, the hydrogenation is unselective even at low conversion, Fig. 5.

Assuming highly crystalline particles with hcp structure, a particle of diameter 1.1 nm would have the vast majority of catalytic surface atoms occupying vertex or edge positions. Such vertex ruthenium atoms **Ru_v**, which under H_2 atmosphere are ligated by hydrides, may coordinate one C=C double bond of **CYD**. The product of the subsequent hydrogenation is **CYE**, which must undergo a second coordination to give the fully hydrogenated **CYA**. Similarly, for a larger particle of average diameter 2.9 nm assuming high crystallinity and an hcp structure, it is evident that most of the catalytically active surface ruthenium atoms are found in facial positions, **Ru_f**. Indeed, here, such crystallinity has already been observed by HREM, Fig. 1. **Ru_f** may hydrogenate the olefin using the mechanism previously discussed, but due to the planar arrangement of **Ru_f**, another mechanism may be envisaged involving the double coordination of the diene, as generally found during the hydrogenation of 1,3-cyclohexadiene on metallic surfaces [46,47], and thus, rapid consecutive hydrogenation of both double bonds leading to the fully hydrogenated **CYA** may be envisaged. In Fig. 6 are represented simplified SYBYL models of **CYD** molecules coordinating to the surface of perfectly crystalline RuNPs of calculated average diameter 1.3 nm and 2.8 nm. This illustrates nicely the greater facility of planar coordination to faces of the larger NPs and could explain the lower selectivity of the larger RuNPs despite identical reaction conditions. Likewise, in the hydrogenation of 1,3-butadiene or 1-hexyne, the selectivity of small NPs towards 1-butene or 1-hexene versus butane or hexane is still higher than that of larger NPs [45–48]. In this work, in the hydrogenation of **CYD**, the selectivity in **CYE** versus **CYA** drops from 97% to 80% when the RuNP size increases from 1.1 to 2.9 nm.

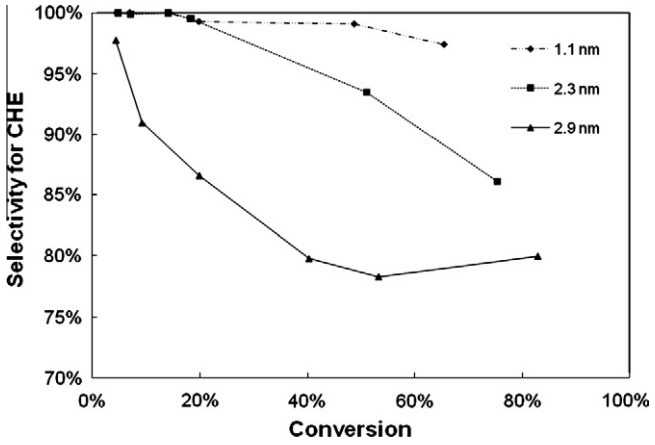

Fig. 5. Selectivity for cyclohexene as a function of conversion for the three different sizes of RuNPs.

Our hypothesis is based on idealised particle shape, which is not likely to exist in reality. Nonetheless, it is widely accepted that large NPs are more likely to present larger open facets where planar π-coordination of diene substrates can occur, whereas small NPs are often reported to be amorphous, therefore presenting no open facets, making this planar coordination even less likely [41].

In studies of CO hydrogenation on RhNPs, the difference in reactivity with size was related to the increasing probability of finding step sites with increasing NP size [49–51]. However, for RuNPs of less than 3 nm, as reported here, calculations have shown that such step sites are not likely to exist [52].

The highly selective hydrogenation of 1,3-cyclohexadiene to cyclohexene has also been performed with PdNPs in organic and IL media [33,53,54]. The high selectivity results from the intrinsic properties of Pd metal and its small NP size [55].

3.9. Hydrogen effect

According to the literature, the hydrogenation of olefins in ILs is often biphasic in its nature [56–59], due to the poor solubility of hydrogen and olefins in these media [60–63]. Therefore, the diffusion process of the substrate or H_2 may limit the rate of hydrogenation.

To find out whether H_2 is in fact a rate-limiting reagent, experiments varying the H_2 pressure are performed. Increasing H_2 pressure to 4 bars in the case of **Ru_0** and **Ru_{50}** is seen to affect neither the activity nor selectivity in a substantial manner, Table 3, Experiments 4 and 5. This is similar to results reported by Dupont's group who observed that the reaction rate **does not** depend on the H_2 pressures in $C_1C_4ImBF_4$ [64].

In parallel, it is generally reported that a higher H_2 concentration should influence the activity of the large rather than small particles, as the H_2 storage capacity is related to the particle volume; therefore, large particles may experience an increase in the availability of subsurface hydrogen [44].

In reality, little difference in activity is observed in either case. This proves that the rate is not dictated by the availability and adsorption of H_2, in agreement with observations of labile surface hydrides on the NP surface [17], but by the mobility and absorption of the substrate [26]. Indeed, it is highly likely that the surface of the NPs is already saturated with adsorbed H_2 at the temperature of the reaction [17].

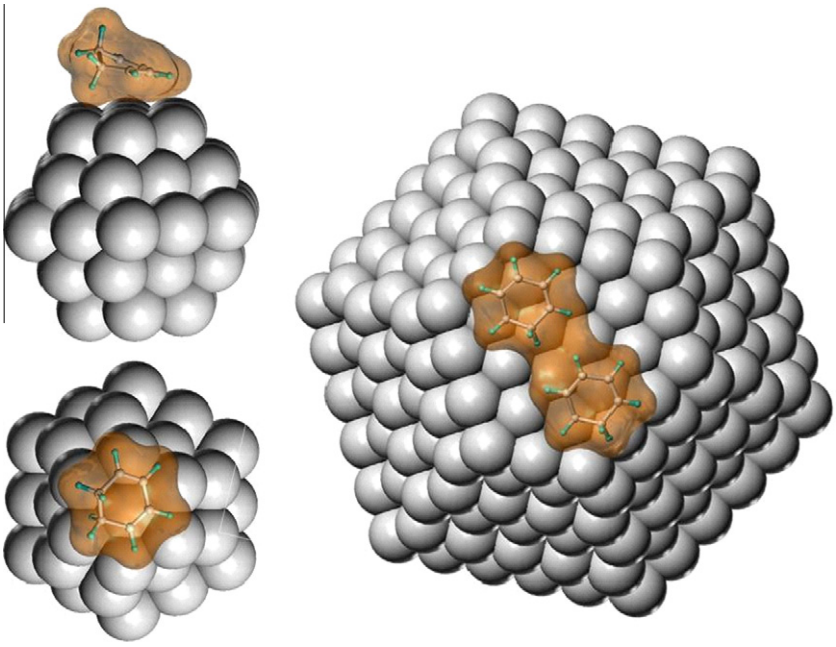

Fig. 6. SYBYL representations of CYD coordinated to the face of highly crystalline RuNPs of mean diameter 1.3 nm (left) and 2.8 nm (right).

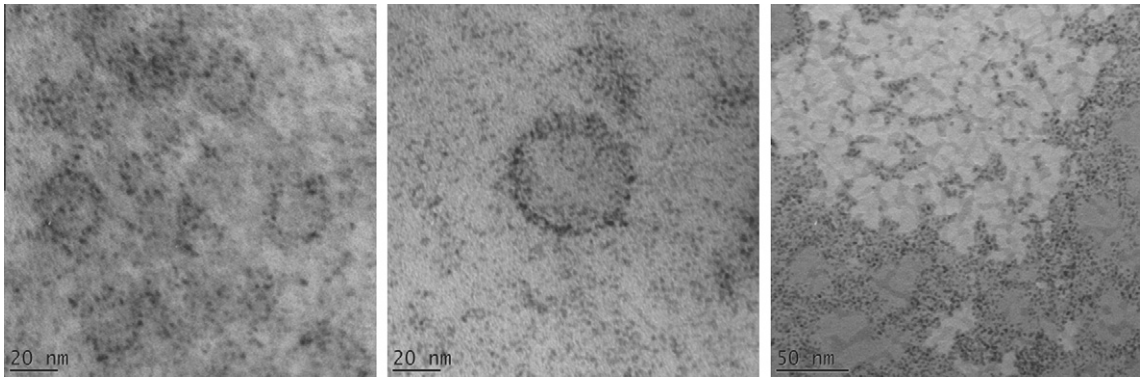

Fig. 7. Transition electron micrographs of RuNPs after CYD hydrogenation for Ru_0 (left), Ru_{25} (middle) and Ru_{50} (right).

Table 5
Recycling of the catalyst **Ru_0**. Conversion, selectivity, turnover number and turnover frequency for the hydrogenation of CYD at 30 °C under 1.2 bar H_2. Products removed under vacuum after each run and analysed by GC.

Experiment number	Cycle	Conversion at 90 min (%)	Selectivity CYE (%)	TON	TOF (h^{-1})	Size after catalysis (nm)
1	1st	66	97	70	46	1.3 ± 0.4
9	2nd	73	95	76	51	–
10	3rd	69	94	73	49	–
11	4th	68	89	71	47	–
12	5th	64	86	67	45	–
13	6th	65	86	68	45	1.8 ± 0.5

3.10. Recycling

TEM images of the reaction medium after hydrogenation, Fig. 7, show that the average size measured (Table 3) does not differ greatly from the original size, in accordance with the stability of RuNPs in ILs under molecular hydrogen [17]; however, the size distribution is larger, probably as an effect of stirring [65].

The apparent resistance to coalescence of the NPs means that they may be tested for their recyclability. Consequently, using the most selective catalyst, **Ru_0**, recycling experiments are performed, by extracting *in vacuo* and quantifying the volatiles after each 90-min run. More **CYD** is then added for hydrogenation. From the results, Table 5 and Fig. 8, it can be seen that both the activity and selectivity remain high after five recycles, diminishing only slightly with each run. This small decrease of course is attributable to the gradual coalescence of the NPs, leading to a diminution in the number of active surface sites and larger, less selective NPs. Indeed, TEM images obtained of the NPs after all recycling

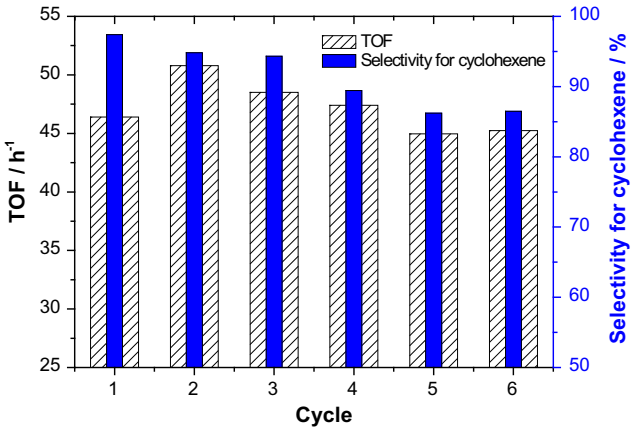

Fig. 8. Evolution of TOF and selectivity with catalyst recycling.

experiments showed that the NPs undergo coalescence to attain an average diameter of 1.8 ± 0.5 nm, approaching the size of **Ru_{25}** and of course presenting a similar selectivity.

4. Conclusion

In this work, the catalytic hydrogenation of 1,3-cyclohexadiene, **CYD**, and cyclohexene, **CYE**, in $C_1C_4ImNTf_2$, was used as a probe for the relationship between size and catalytic performance of RuNPs.

Firstly, tailor-made, size-controlled and zero-valent RuNPs (1–3 nm) were generated from the decomposition of [Ru(COD)(COT)] under H_2 in $C_1C_4ImNTf_2$, by varying the experimental conditions. RuNPs were fully characterised *in situ* by TEM and HREM to determine their sizes and demonstrate their degree of crystallinity and *ex situ* by XPS to verify their zero oxidation state.

Secondly, all catalytic reaction compositions were carefully calculated in order that all parameters except particle size were maintained constant, i.e. **Ru_s** concentration, **CYD**/**Ru_s** ratio and **CYD**/**IL** ratio, the latter governing solvation phenomena and mass transfer factors (viscosity and diffusivity). It was found that for catalytic hydrogenations of **CYD** and **CYE**, the activity of catalyst increases with the NP size in agreement with the literature results on heterogeneous catalysts. In contrast to activity, in the hydrogenation of **CYD**, the selectivity for **CYE** versus **CYA** drops from 97% to 80% when the RuNP size increases from 1.1 to 2.9 nm.

Both results, activity and selectivity, are in agreement with a mechanism involving a π-bond activation and a double coordination of diene substrates, necessitating several neighbouring surface atoms only found in facial positions on the larger NPs. Furthermore, these RuNPs show a high level of recyclability with neither loss of activity nor significant agglomeration.

To conclude, in olefin hydrogenation by ruthenium nanoparticles in ionic liquid media, both reactivity and selectivity are significantly dependent on the nanoparticle size.

Acknowledgments

P.S.C. acknowledges the Ph.D. grant attributed by the Ministère de l'Enseignement Supérieur et de la Recherche, France, and the EU transnational access programme. A.P. thanks the post-doctoral grant by the project ANR CALIST. This work has been funded by CNRS and ANR (ANR Project CALIST, ANR-07-CP2D-02-03).

Appendix A. Supplementary data

Supplementary data associated with this article can be found, in the online version, at doi:10.1016/j.jcat.2010.07.018.

References

[1] M. Valden, X. Lai, D.W. Goodman, Science 281 (1998) 1647.
[2] A.T. Bell, Science 299 (2003) 1688–1691.
[3] G. Schmid, Nanoparticles: From Theory to Application, Wiley-VCH, Weinheim, 2004.
[4] K. Lee, M. Kim, H. Kim, J. Mater. Chem. 20 (2010) 3791–3798.
[5] A.Z. Moshfegh, J. Phys. D: Appl. Phys. 42 (2009) 233001. 233032.
[6] G.A. Somorjai, J.Y. Park, Top. Catal. 49 (2008) 126–135.
[7] H. Boennemann, K.S. Nagabhushana, in: B. Corain, G. Schmid, N. Toshima (Eds.), Metal Nanoclusters in Catalysis and Materials Science: The Issue of Size Control, Elsevier B.V., Amsterdam, pp. 21–48.
[8] H. Bönnemann, K.S. Nagabhushana, R.M. Richards, in: D. Astruc (Ed.), Nanoparticles and Catalysis, Wiley-VCH, Weinheim, 2008, pp. 49–92.
[9] H. Tada, T. Kiyonaga, S. Naya, Chem. Soc. Rev. 38 (2009) 1849.
[10] D. Astruc, Nanoparticles and Catalysis, Wiley-VCH, Weinheim, 2008.
[11] J. Dupont, J.D. Scholten, Chem. Soc. Rev. 39 (2010) 1780–1804.
[12] J. Dupont, Nanoparticles and Catalysis, Wiley-VCH, Weinheim.
[13] T. Gutel, C.C. Santini, K. Philippot, A. Padua, K. Pelzer, B. Chaudret, Y. Chauvin, J.-M. Basset, J. Mater. Chem. 19 (2009) 3624–3631.
[14] A.A.H. Padua, M.F. Costa Gomes, J.N.A. Canongia Lopes, Acc. Chem. Res. 40 (2007) 1087–1096.
[15] J.N. Canongia Lopes, M.F. Costa Gomes, A.A.H. Padua, J. Phys. Chem. B 110 (2006) 16816–16818.
[16] T. Gutel, J. Garcia-Anton, K. Pelzer, K. Philippot, C.C. Santini, Y. Chauvin, B. Chaudret, J.-M. Basset, J. Mater. Chem. 17 (2007) 3290–3292.
[17] P.S. Campbell, C.C. Santini, D. Bouchu, B. Fenet, K. Philippot, B. Chaudret, A.A.H. Padua, Y. Chauvin, Phys. Chem. Chem. Phys. 12 (2010) 4217–4223.
[18] C. Vollmer, E. Redel, K. Abu-Shandi, R. Thomann, H. Manyar, C. Hardacre, C. Janiak, Chem. Eur. J. 16 (2010) 3849–3858. S3849/3841-S3849/3834.
[19] E. Redel, J. Kraemer, R. Thomann, C. Janiak, J. Organometal. Chem. 694 (2009) 1069–1075.
[20] M.H.G. Prechtl, J.D. Scholten, J. Dupont, J. Mol. Catal. A 313 (2009) 74–78.
[21] B. Leger, A. Denicourt-Nowicki, H. Olivier-Bourbigou, A. Roucoux, Inorg. Chem. 47 (2008) 9090–9096.
[22] P. Wasserscheid, T. Welton, Ionic Liquids in Synthesis, Wiley-VCH, Weinheim, 2008.
[23] H. Olivier-Bourbigou, C. Vallee, Multiphase Homogeneous Catalysis, Wiley-VCH, Weinheim, pp. 413–431.
[24] J. Dupont, P.A.Z. Suarez, R.F. De Souza, R.A. Burrow, J.-P. Kintzinger, Chem. Eur. J. 6 (2000) 2377–2381.
[25] J. Lachwa, I. Bento, M.T. Duarte, J.N.C. Lopes, L.P.N. Rebelo, Chem. Commun. (2006) 2445–2447.
[26] T. Gutel, C.C. Santini, A.A.H. Padua, B. Fenet, Y. Chauvin, J.N. Canongia Lopes, F. Bayard, M.F. Costa Gomes, A.S. Pensado, J. Phys. Chem. B 113 (2009) 170–177.
[27] P.S. Campbell, A. Podgorsek, T. Gutel, C.C. Santini, A.A.H. Padua, M.F. Costa Gomes, F. Bayard, B. Fenet, Y. Chauvin, J. Phys. Chem. B 114 (2010) 8156–8165.
[28] A. Mele, G. Romano, M. Giannone, E. Ragg, G. Fronza, G. Raos, V. Marcon, Angew. Chem. Int. Ed. 45 (2006) 1123–1126.
[29] A. Triolo, O. Russina, H.-J. Bleif, E. Di Cola, J. Phys. Chem. B 111 (2007) 4641–4644.
[30] L. Magna, Y. Chauvin, G.P. Niccolai, J.-M. Basset, Organometallics 22 (2003) 4418–4425.
[31] P. Pertici, G. Vitulli, Inorg. Synth. 22 (1983) 176–181.
[32] Y. Chauvin, S. Einloft, B.H. Olivier, Ind. Eng. Chem. Res. 34 (1995) 1149–1155.
[33] J. Huang, T. Jiang, B. Han, H. Gao, Y. Chang, G. Zhao, W. Wu, Chem. Commun. (2003) 1654–1655.
[34] A.P. Umpierre, G. Machado, G.H. Fecher, J. Morais, J. Dupont, Adv. Synth. Catal. 347 (2005) 1404–1412.
[35] E.T. Silveira, A.P. Umpierre, L.M. Rossi, G. Machado, J. Morais, G.V. Soares, I.J.R. Baumvol, S.R. Teixeira, P.F.P. Fichtner, J. Dupont, Chem. Eur. J. 10 (2004) 3734–3740.
[36] K. Philippot, B. Chaudret, C.R. Chimie 6 (2003) 1019–1034.
[37] N. Bedford, C. Dablemont, G. Viau, P. Chupas, V. Petkov, J. Phys. Chem. C 111 (2007) 18214–18219.
[38] R. Nyholm, N. Martensson, J. Phys. Chem. 13 (1980) L279.
[39] J.A. Van Bokhoven, J.T. Miller, J. Phys. Chem. C 111 (2007) 9245.
[40] V.A. Finkel, M.I. Palatnik, G.P. Kovtun, Phys. Met. Metall. 32 (1971) 231.
[41] R.A. Van Santen, Acc. Chem. Res. 42 (2009) 57–66.
[42] A. Denicourt-Nowicki, A. Ponchel, E. Monflier, A. Roucoux, Dalton Trans. 48 (2007) 5714–5719.
[43] D.Y. Murzin, Chem. Eng. Sci. 64 (2009) 1046–1052.
[44] A. Binder, M. Seipenbusch, M. Muhler, G. Kasper, J. Catal. 268 (2009) 150–155.
[45] N. Semagina, A. Renken, L. Kiwi-Minsker, J. Phys. Chem. C 111 (2007) 13933–13937.
[46] M. Saeys, M.-F. Reyniers, M. Neurock, G.B. Marin, Surf. Sci. 600 (2006) 3121–3134.
[47] W.L. Manner, G.S. Girolami, R.G. Nuzzo, J. Phys. Chem. B 102 (1998) 10295–10306.
[48] J. Silvestre-Albero, G. Rupprechter, H.-J. Freund, J. Catal. 240 (2006) 58–65.
[49] H. Arakawa, K. Takeuchi, T. Matsuzaki, Y. Sugi, Chem. Lett. 13 (1984) 1607.
[50] T. Hanaoka, H. Arakawa, T. Matsuzaki, Y. Sugi, K. Kanno, Y. Abe, Catal. Today 58 (2000) 271.
[51] S. Zhou, H. Zhao, D. Ma, S. Miao, M. Cheng, X. Bao, Z. Phys. Chem. 219 (2005) 949.
[52] J. Gavnholt, J. Schiotz, Phys. Rev. B 77 (2008) 035404/035401–035404/035410.
[53] M.V. Seregina, L.M. Bronstein, O.A. Platonova, D.M. Chernyshov, P.M. Valetsky, J.r. Hartmann, E. Wenz, M. Antonietti, Chem. Mater. 9 (1997) 923.

[54] J. Huang, T. Jiang, H. Gao, B. Han, Z. Liu, W. Wu, Y. Chang, G. Zhao, Angew. Chem. Int. Ed. 43 (2004) 1397–1399.
[55] G. Ertl, H. Knozinger, J. Weitkamp (Eds.), Handbook of Heterogeneous Catalysis, Wiley-VCH, Weinheim, 1997.
[56] J. Dupont, G.S. Fonseca, A.P. Umpierre, P.F.P. Fichtner, S.R. Teixeira, J. Am. Chem. Soc. 124 (2002) 4228–4229.
[57] P.J. Dyson, Appl. Organomet. Chem. 16 (2002) 495–500.
[58] P.J. Dyson, in: a.M.T.J. Mc Cleverty (Ed.), Comprehensive Coordination Chemistry II, Elsevier, Amsterdam, pp. 557–566.
[59] P.J. Dyson, D. Zhao, Multiphase Homogeneous Catalysis, Wiley-VCH, Weinheim, pp. 494–511.
[60] P.J. Dyson, G. Laurenczy, C.A. Ohlin, J. Vallance, T. Welton, Chem. Commun. (2003) 2418–2419.
[61] J. Jacquemin, M.F. Costa Gomes, P. Husson, V. Majer, J. Chem. Thermodyn. 38 (2006) 490–502.
[62] J. Jacquemin, P. Husson, V. Majer, M.F. Costa Gomes, Fluid Phase Equilib. 240 (2006) 87.
[63] J. Jacquemin, P. Husson, V. Majer, M.F. Costa Gomes, J. Solution Chem. 36 (2007) 967–979.
[64] P. Migowski, D. Zanchet, G. Machado, M.A. Gelesky, S.r.R. Teixeira, J. Dupont, Phys. Chem. Chem. Phys. 12 (2010) 6826–6833.
[65] D. Li, R.B. Kaner, J. Am. Chem. Soc. 128 (2006) 968–975.